Multiscale reverse engineering of the human ocular surface

Jeongyun Seo[1], Woo Y. Byun [1], Farid Alisafaei[2], Andrei Georgescu [1], Yoon-Suk Yi[1], Mina Massaro-Giordano[3,4], Vivek B. Shenoy[2,5], Vivian Lee[3], Vatinee Y. Bunya[3,4] and Dongeun Huh [1,5,6]*

[1]Department of Bioengineering, University of Pennsylvania, Philadelphia, PA, USA. [2]Department of Materials Science and Engineering, University of Pennsylvania, Philadelphia, PA, USA. [3]Department of Ophthalmology, Scheie Eye Institute, Perelman School of Medicine, University of Pennsylvania, Philadelphia, PA, USA. [4]Penn Dry Eye and Ocular Surface Center, Perelman School of Medicine, University of Pennsylvania, Philadelphia, PA, USA. [5]NSF Science and Technology Center for Engineering Mechanobiology, University of Pennsylvania, Philadelphia, PA, USA. [6]Institute for Regenerative Medicine, Perelman School of Medicine, University of Pennsylvania, Philadelphia, PA, USA. *e-mail: huhd@seas.upenn.edu

Supplementary Information (SI) Guide for

Multiscale Reverse Engineering of the Human Ocular Surface

Jeongyun Seo, Woo Y. Byun, Farid Alisafaei, Andrei Georgescu, Yoon-Suk Yi, Mina Massaro-Giordano, Vivek B. Shenoy, Vivian Lee, Vatinee Y. Bunya, Dongeun Huh*

Supplementary Information includes:

Supplementary Methods
- Fabrication of device layers
- Production of cell culture scaffolds
- Device assembly
- Formation of sub-epithelial stroma
- Fabrication of biomimetic eyelids
- Coupling and operation of electromechanical actuator
- Digitally controlled dry eye disease (DED) simulation platform
- Tear osmolarity measurement
- Videokeratography
- Mathematical modeling of blink-induced mechanical forces

Supplementary Table: list of primary and secondary antibodies used.

Supplementary Videos 1 to 3
Supplementary Video 1 shows the key components of the engineered human ocular surface model and demonstrates how eye blinking and tear film formation are simulated in the device.

Supplementary Video 2 shows a top-down view of a hydrogel eyelid (blue) sliding over the engineered ocular surface. The eyelid is actuated at 0.2 Hz to match the frequency of physiological spontaneous blinking in the human eye. The movie is played in real time.

Supplementary Video 3 shows the digitally controlled DED simulation platform depicted in **Supplementary Methods: Digitally controlled dry eye disease (DED) simulation platform**. The entire system is set up in a temperature-controlled cell culture incubator that contains a computer-controlled humidity sensor and humidifier to regulate the relative humidity of air in the surrounding environment of the DED model. The engineered device is mounted vertically on a custom-designed stage equipped with a heating pad and temperature probe. Two programmable syringe pumps are connected to the access ports of the device to perfuse the culture chamber with media and to inject artificial tears into the tear channel. The movie is played in real time.

Supplementary Methods

Fabrication of device layers

Our engineered cell culture device consists of two elastomeric layers and a dome-shaped cell culture scaffold. The upper layer contains an open well that provides direct access to the scaffold and guides the movement of a biomimetic eyelid during blinking actuation. The lower layer has two fluidic channels including a perfusion chamber for cell culture and a tear channel for delivery and controlled release of tear fluid. The upper and lower layers were fabricated by casting poly(dimethylsiloxane) (PDMS) against 3D-printed plastic (Accura SL 5530) masters. Briefly, PDMS base (Sylgard® 184 silicone elastomer, Dow Corning) was mixed with a curing agent at a weight ratio of 10:1 (base:curing agent) and degassed in a desiccating chamber for 1 hour to remove air bubbles. The mixed PDMS was then poured onto a master for the upper layer containing a 3D-printed protrusion that defined the shape and size of the open well. Importantly, the master also included additional features to create a bubble trap for the perfusion chamber and a drainage channel designed to receive and drain excess tears during blinking in our model. The master filled with PDMS was then covered and pressed against a flat plastic plate to ensure surface flatness of the resultant structure.
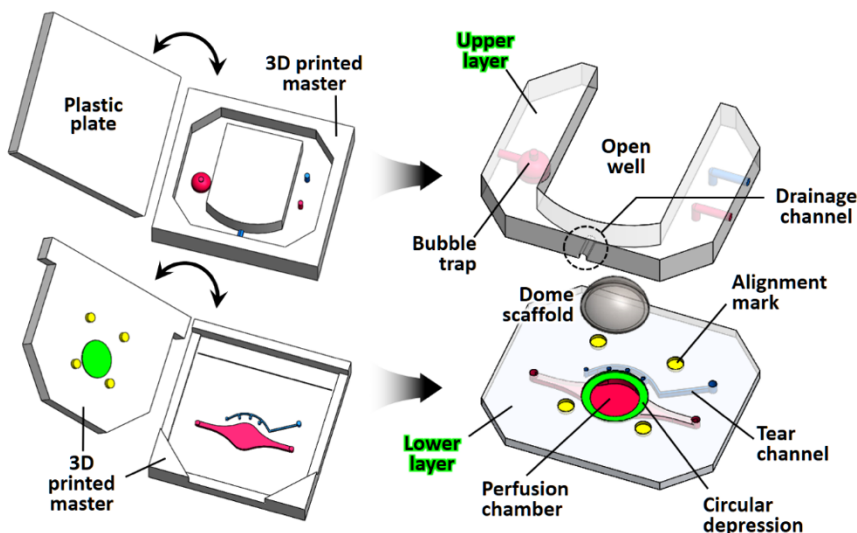

To fabricate the lower layer, degassed PDMS pre-polymer was dispensed into a 3D-printed master patterned with protruding features of the perfusion chamber and tear channel. After complete filling and spreading, the master was covered with another 3D-printed master that contained positive relief patterns used to create a circular depression and four alignment marks on the surface of the lower PDMS layer for scaffold bonding and 3D cell patterning (see **Supplementary Methods: Device assembly** and **Extended Data Figure 1. Formation of corneal and conjunctival epithelia using 3D cell patterning technique** for more information).

After curing PDMS at 65 ºC for at least 3 hours, the hardened upper and lower PDMS slabs were peeled off of their respective masters. We then used a 1 mm biopsy punch to generate sideway holes in the upper layer that served as access ports to the bubble trap, perfusion chamber, and tear channel. In the lower layer, biopsy punches were used to create i) open 0.5 mm orifices in the tear channel, ii) 1 mm holes for the inlet and outlet of the perfusion chamber that were connected to the access ports in the upper layer, and iii) the perfusion chamber with a diameter of 6 mm. The lower PDMS slab was then treated with air plasma, bonded to a glass slide, and incubated at 65 ºC overnight to achieve permanent bonding. Subsequently, the upper PDMS slab was bonded to the lower layer to create a multilayered device ready for integration with the dome-shaped cell culture scaffold.

Production of cell culture scaffolds

The dome-shaped 3D cell culture scaffolds used in our model were generated by compression molding of commercially available thin and microporous polystyrene cell culture substrates (Alvetex®, Reprocell). Briefly, we used a 3D printer (Protolabs) to fabricate a pair of complementary concave and convex plastic molds whose radius of curvature closely matched that of the human cornea (7 mm). For the production of dome scaffolds, a 200 µm-thick planar Alvetex substrate was sandwiched between the 3D-printed molds and then heated for 15 minutes in a convection oven (Quincy Lab, Inc.) maintained at 100 °C to induce permanent deformation. A 200 µm-thick Kapton sheet (DuPont) was used as a spacer to prevent complete collapse of the sandwiched scaffold during compression. Finally, the assembly was cooled to room temperature, after which the molds and protective films were removed to release a dome-shaped scaffold.
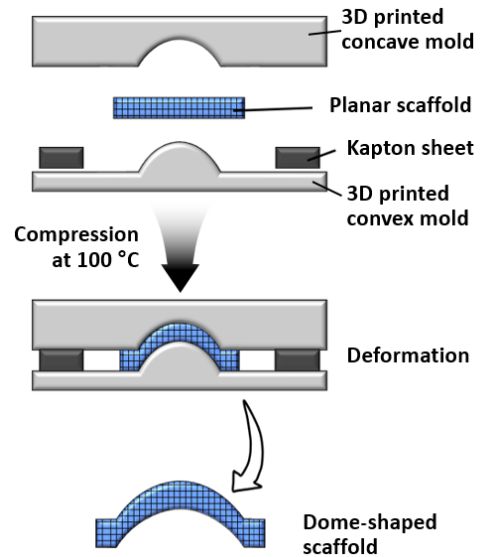

Device assembly
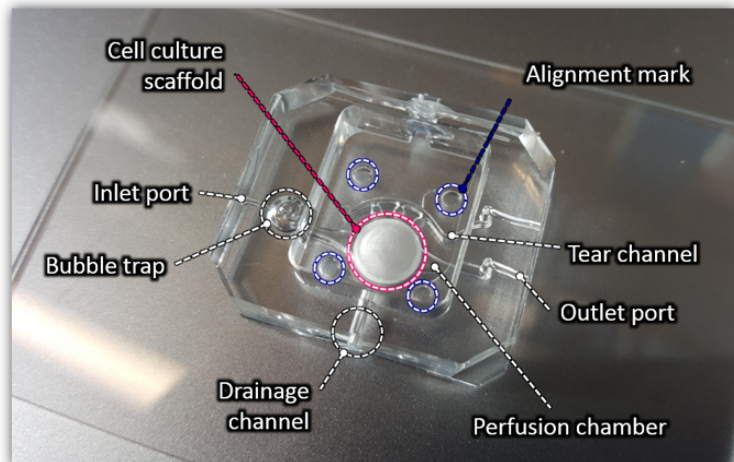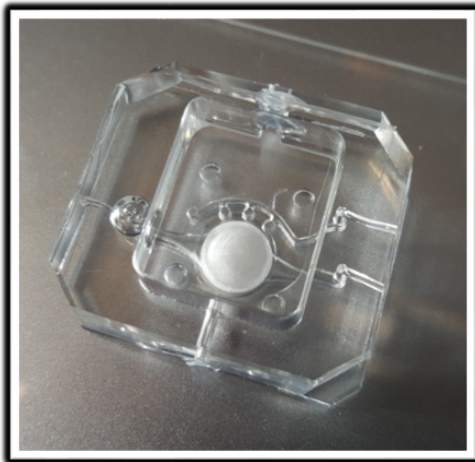
In the first step of device assembly, the dome scaffold was bonded to the lower PDMS layer described above. To achieve bonding, a pre-polymer of PDMS and a curing agent were mixed at a weight ratio of 10:1 (PDMS:curing agent) and spin-coated on a glass substrate at 1200 rpm for 5 minutes. Subsequently, the cell culture scaffold was gently placed on the spin-coated layer to wet the flat base of the scaffold with uncured PDMS. After curing at 45 ºC for at least 3 hours, the outer edge of the base was trimmed away using a biopsy punch to make the final diameter of the scaffold 7 mm. The trimmed scaffold was then stamped on a thin layer of uncured PDMS prepared using the same spin-coating method, bonded to a circular depression on the surface of the lower PDMS slab, and baked overnight at 45 ºC. The assembled device is shown in the photo above. Finally, blunt needles (Kimble) were inserted into the inlet and outlet ports of the device to provide fluidic access to the perfusion chamber and tear channel.

Formation of sub-epithelial stroma

Prior to cell seeding, the assembled device was sterilized with 70% ethanol and thoroughly rinsed with deionized water. The scaffold was then incubated overnight with a phosphate-buffered saline (PBS) solution containing human-derived fibronectin (Corning®) (0.04 mg/ml). To generate a stromal layer in the scaffold, primary human keratocytes were trypsinized and suspended in a solution prepared by mixing rat tail type 1 collagen (2 mg/ml) with deionized water, 10X PBS, and 1N NaOH. The final concentration of suspended cells was 1 million cells/ml. In the next step, 25 µl of this cell-containing collagen precursor solution was dispensed on the scaffold surface and then drawn into the pores of the scaffold by gentle aspiration applied to the outlet of the underlying perfusion chamber. Gelation of collagen was achieved by incubating the seeded device in a humidified cell culture incubator (37 °C, 5% CO_2) for 30 minutes. The cells embedded in the collagen gel were cultured for 3 days before seeding of epithelial cells by adding keratocyte growth medium into the open well in the upper PDMS layer and also flowing it through the perfusion chamber in the lower layer.
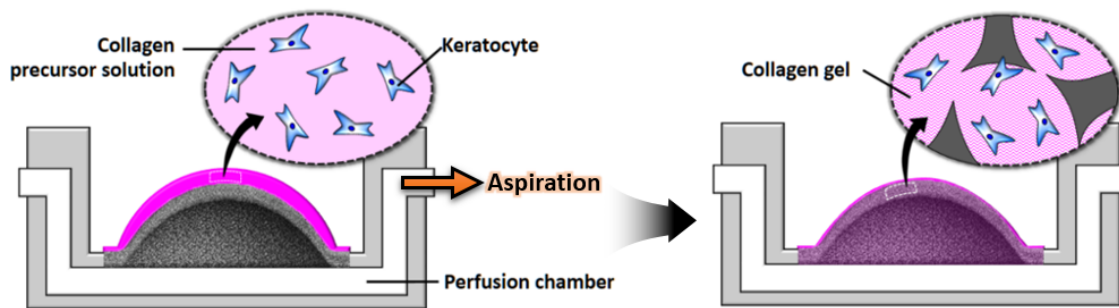
Fabrication of biomimetic eyelids

The eyelids were produced by casting and crosslinking gelatin methacryloyl (gel-MA) with ultraviolet (UV) light. To accomplish this, a gel-MA solution was prepared by dissolving lyophilized gel-MA powder in PBS at a final concentration of 17.5% w/v at 65 °C for 20 minutes with interrupted vortexing every 5 minutes. In parallel, a photoinitiator solution was prepared by mixing lithium arylphosphonate (LAP, Allevi) with PBS at 1% w/v followed by heating at 65 °C until LAP was completely dissolved. The gel-MA solution was then mixed with an equal volume of 1% LAP solution. The 1:1 mixture of gel-MA and LAP was briefly heated up to 90 °C to reduce the viscosity of the solution and sterile-filtered (Millex® Syringe Filters, EMD Millipore). The sterile gel-MA solution was then cooled to 37 °C.
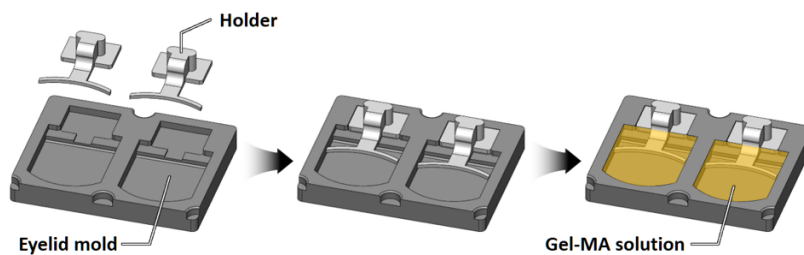
For fabrication of the eyelids, we 3D-printed eyelid molds and arc-shaped holders designed to connect the hydrogel eyelid to a computer-controlled electromechanical actuator. Prior to hydrogel casting, the printed parts were sterilized with 70% ethanol and dried in a sterile biosafety cabinet. The molds were then rinsed with 3% bovine serum albumin (BSA) solution to wet the surfaces as a way to prevent the formation of air bubbles during the introduction of hydrogel solution. After the BSA solution was

aspirated, the 3D-printed sterile eyelid holders were inserted into the molds. Subsequently, 200 μl of gel-MA solution was dispensed into each mold to fill the entire cavity with a thickness of 1 mm and to submerge the arc-portion of the eyelid holder. The hydrogel solution-containing assembly was then transferred to a UV box (ELC-500 UV Curing Chamber, Electro-Lite Corporation). Cross-linking of gel-MA was achieved by exposing the solution to UV for 48 seconds at 30 mW/cm^2, and the complete eyelids were carefully removed from the molds and incubated in PBS at 65 ºC for 30 minutes to eliminate any bubbles. Afterwards, the eyelids were cooled down to room temperature, transferred to cell culture medium, and stored at 4 ºC until use.

Coupling and operation of electromechanical actuator
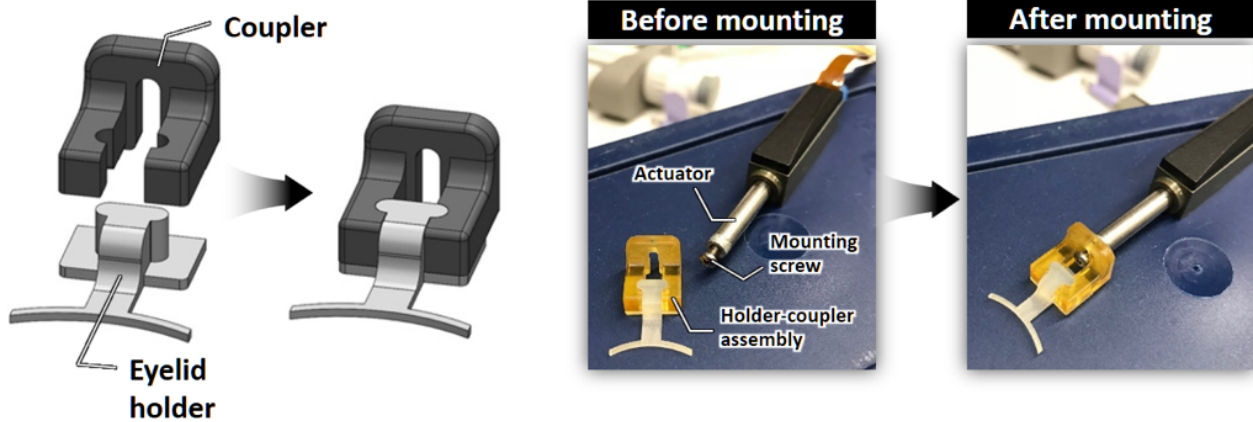
A computer-controlled electromechanical system was constructed using a linear micromotor (Faulhaber GmbH) to actuate the movement of the hydrogel eyelid. To connect the actuator to the eyelid, we designed and 3D-printed a plastic coupler shown in the figure below having a complementary shape to the eyelid holder. Mounting of the actuator was achieved by first clipping the eyelid holder into the coupler and then connecting the axial mounting screw of the linear micromotor shaft to the coupler. The assembled actuator unit was powered and operated by a Faulhaber linear motor controller. Motor command was performed by USB connection using Faulhaber Motion Manager software.

Digitally controlled dry eye disease (DED) simulation platform

The DED simulation platform was constructed in a water-jacketed temperature-controlled cell culture incubator (Forma™ Steri-Cycle™ CO2 Incubator, Thermo Fisher) augmented with a humidity control system. To achieve feedback-based regulation of relative humidity in the platform, a water pan in the bottom of the incubator was removed and replaced with an ultrasonic humidifier (Boneco) capable of vaporizing sterile deionized water into the air until desired relative humidity (RH) was reached. The RH inside the DED simulation platform was constantly monitored by a digital humidity sensor (SHT15, Sparkfun) connected to an Arduino microcontroller (Arduino Due). When the RH fell below a threshold, which was set at 1% lower than the desired level, the Arduino microcontroller was programmed to activate the humidifier to generate water vapor until the humidity reached the level that was 1% higher than the target humidity. This feedback control was used to maintain the RH in the DED chamber at 50% in order to approximate the RH of air at moderate ambient temperatures.
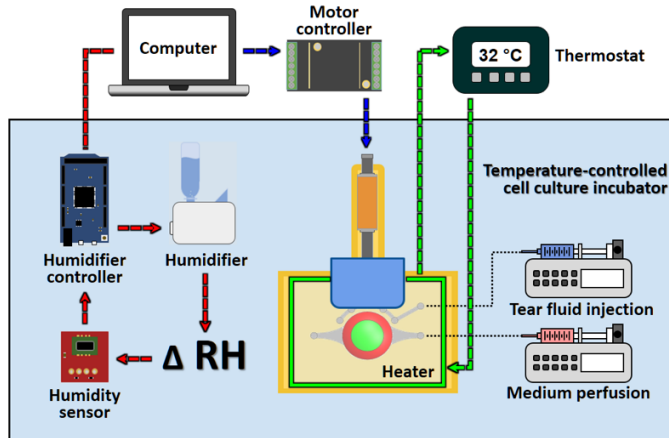
During DED experiments, the temperature of the incubator was fixed at 25 °C but our device was kept on a polyimide film heater (Kapton® Insulated Flexible Heaters, Omega), which was connected to a digital thermostat (Digital Thermostat, Willhi). This active heating system, which was designed to monitor and adjust the power of the heater through negative feedback control, maintained the temperature of culture medium in our device at 32 °C.

Tear osmolarity measurement
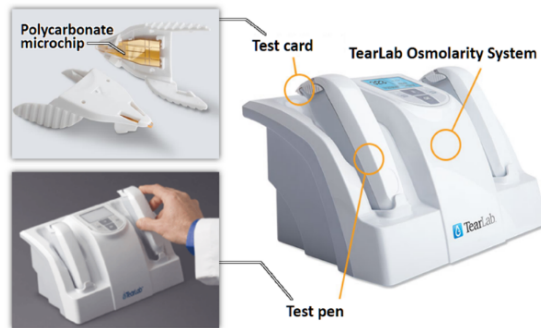
The osmolarity of tear fluid in the eye model was determined using the TearLab™ Osmolarity System (TearLab™ Corp.). The TearLab system consists of a digital reader and a hand-held measuring apparatus (test pen) that contained a disposable polycarbonate microchip (test card) designed for rapid collection of tear fluid. Prior to measurement, the system calibration was validated using reference tear solutions provided by the manufacturer.

To evaluate tear osmolarity in our model, we first stopped blinking actuation at the open position and placed the tip of test card on the tear film meniscus at the edge of the eyelid to sample 50 nl of tears by capillary action. The test pen was then docked into the reader, and the digital reading on the display of the instrument was recorded to document tear osmolarity. The osmolarity of our cell culture medium and unconditioned fresh tears was below 275 mOsms/L.

Videokeratography
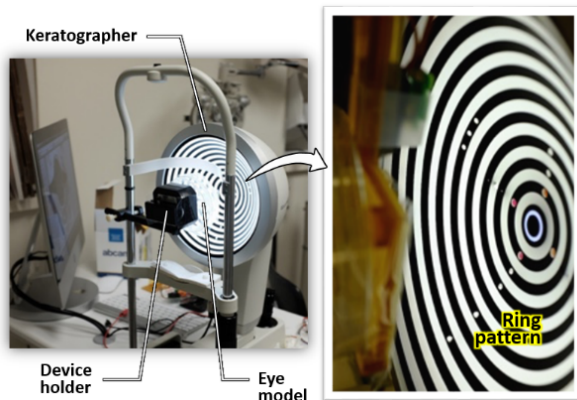
The stability of the tear film was measured using the OCULUS Keratograph® 5M (OCULUS, Inc.). Prior to imaging, purple dye was injected into the perfusion chamber to enhance the contrast of the scaffold. The eye model was then mounted vertically on the keratographer using a custom-designed device holder as shown at left. Subsequently, an illuminated pattern of concentric rings on the concave chamber of the keratographer was projected onto the engineered ocular surface. Once a stable pattern was detected, the eyelid was actuated to blink once, after which the entire ocular surface was video-recorded using a built-in camera to monitor the stability of individual rings.

Temporal stability of the tear film was determined by analysis of videokeratographs as captured by the OCULUS Keratograph platform. Briefly, we used ImageJ to segment videokeratographs into radial sectors and for each sector, to determine the video frame and thus the time at which tear film break-up occurred. The instability and break-up of the tear film caused sudden, ripple-like distortions of the reflected concentric ring pattern. Since the occurrence of rippling and blurring or disruption of the high-contrast ring pattern was sufficiently rapid and pronounced that its sector-by-sector initiation was often localized to a single video frame. Therefore, we conducted frame-by-frame analysis of spatial variations in pixel intensity due to tear film break-up-induced distortion of the keratographs. If the breakup occurred over multiple frames (typically 3 frames maximum), the median frame number was used. The frame number was then converted to time in seconds by using the frame rate of the keratography camera (10 frames/s). In this analysis, we used videokeratographs recorded for 15 seconds after a blink motion. The fractional area of tear film instability shown in **Figures 4f, 5f** was determined by dividing the number of sectors with a tear film break-up time of 3 seconds or less by the total number of sectors.

Mathematical modeling of blink-induced mechanical forces
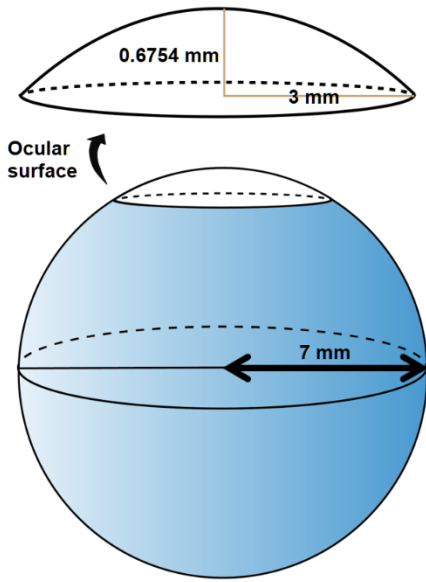
A theoretical elasto-hydrodynamic model was developed and used to show the capability of our experimental system to recapitulate the physiological levels of mechanical forces acting on the human ocular surface during spontaneous blinking. Our mathematical model allowed for predictions of (i) the pressure developed in the tear film, (ii) the normal and shear stresses acting on the ocular surface, and (iii) the resulting deformations of the ocular surface during blinking. As shown in **Fig. 3g**, the elasto-hydrodynamic model includes (i) the ocular surface, (ii) the eyelid, and (iii) the tear film, which are described in detail in the following sections.

1. Ocular Surface

We considered the engineered ocular surface as a deformable body in our mathematical model. The diagram at left shows the three-dimensional geometry of the engineered ocular surface in our experimental model. We treated the ocular surface as a nonlinear material using a neo-Hookean hyper-elastic model. The strain energy density for a neo-Hookean material can be defined as[1]

$$W = \frac{\mu_{\text{ocular}}}{2}(\bar{I}_1 - 3) + \frac{K_{\text{ocular}}}{2}(J - 1)^2 \tag{1}$$

where μ_{ocular} and K_{ocular} are the shear and bulk moduli, respectively, which are related to the Young's modulus E_{ocular} and the Poisson's ratio v_{ocular} as follows.

$$\mu_{\text{ocular}} = \frac{E_{\text{ocular}}}{2(1 + v_{\text{ocular}})} \quad , \quad K_{\text{ocular}} = \frac{E_{\text{ocular}}}{3(1 - 2v_{\text{ocular}})} \tag{2}$$

In Eq. (1), $J = \det(\mathbf{F})$ is the Jacobian of the deformation gradient tensor $\mathrm{F}_{ij} = \partial x_i / \partial X_j$ where x and X denote the current and reference configurations, respectively. The deformation gradient

tensor $\mathbf{F}$ is multiplicatively split as $\mathbf{F} = \mathbf{F}_v \mathbf{F}_{\text{iso}} = \mathbf{F}_{\text{iso}} \mathbf{F}_v$ where $\mathbf{F}_v = J^{1/3}\mathbf{I}$ and $\mathbf{F}_{\text{iso}} = J^{-1/3}\mathbf{F}$ are the volumetric and isochoric (volume-preserving) components of $\mathbf{F}$, respectively ($\mathbf{I}$ is the second-order identity tensor). With the above decomposition at hand, $\bar{I}_1$ in Eq. (1) is defined as the first strain invariant of $\mathbf{B}_{\text{iso}}$ and $\mathbf{C}_{\text{iso}}$ tensors

$$\bar{I}_1 = \text{tr}(\mathbf{B}_{\text{iso}}) = \text{tr}(\mathbf{C}_{\text{iso}}) \tag{3}$$

where

$$\mathbf{B}_{\text{iso}} = \mathbf{F}_{\text{iso}}\mathbf{F}_{\text{iso}}^T = J^{-2/3}\mathbf{B} \tag{4}$$

is the isochoric left Cauchy-Green strain tensor, and

$$\mathbf{C}_{\text{iso}} = \mathbf{F}_{\text{iso}}^T\mathbf{F}_{\text{iso}} = J^{-2/3}\mathbf{C} \tag{5}$$

is the isochoric right Cauchy-Green strain tensor[2]. The left and right Cauchy-Green strain tensors $\mathbf{B} = \mathbf{F}\mathbf{F}^T$ and $\mathbf{C} = \mathbf{F}^T\mathbf{F}$ can be defined in terms of the principal stretches λ_1, λ_2, and λ_3 via the spectral representation

$$\mathbf{B} = \sum_{a=1}^{3} \lambda_a^2\, \boldsymbol{n}_a \otimes \boldsymbol{n}_a \quad , \qquad \mathbf{C} = \sum_{a=1}^{3} \lambda_a^2\, \boldsymbol{N}_a \otimes \boldsymbol{N}_a \tag{6}$$

where the orthogonal vectors $\boldsymbol{N}_a$ and $\boldsymbol{n}_a = \mathbf{R}\,\boldsymbol{N}_a$ (with $a = 1,2,3$) are respectively the unit vectors in the principal stretch directions for the reference and current configurations, $\mathbf{R}$ is the orthogonal rotation tensor, and $\otimes$ represents the dyadic product of two arbitrary vectors $\boldsymbol{u}$ and $\boldsymbol{v}$ as $(\boldsymbol{u} \otimes \boldsymbol{v})_{ij} = u_i v_j$. Using the strain energy density function in Eq. (1), the Cauchy stress tensor $\boldsymbol{\sigma}$ and the consistent Jacobian elasticity tensor $\mathbb{C}$ are defined as

$$\boldsymbol{\sigma} = \frac{\mu_{\text{ocular}}}{J}\left(\mathbf{B}_{\text{iso}} - \frac{1}{3}\text{tr}(\mathbf{B}_{\text{iso}})\mathbf{I}\right) + K_{\text{ocular}}(J-1)\mathbf{I} \tag{7}$$

$$\begin{aligned}
\mathbb{C}_{ijkl} &= \frac{1}{J}\frac{\partial \Delta(J\boldsymbol{\sigma})}{\partial \Delta\boldsymbol{\varepsilon}} \\
&= \frac{\mu_{\text{ocular}}}{J}\left(\frac{1}{2}\left(\delta_{ik}\bar{B}_{jl} + \bar{B}_{ik}\delta_{jl} + \delta_{il}\bar{B}_{jk} + \bar{B}_{il}\delta_{jk}\right) - \frac{2}{3}\left(\delta_{ij}\bar{B}_{kl} + \bar{B}_{ij}\delta_{kl}\right) + \frac{2}{9}\delta_{ij}\delta_{kl}\bar{B}_{mm}\right) \\
&\quad + K_{\text{ocular}}(2J-1)\delta_{ij}\delta_{kl}
\end{aligned} \tag{8}$$

where $\bar{\mathbf{B}} = \mathbf{B}_{\text{iso}}$ and δ_{ij} is the Kronecker delta. The above constitutive law was implemented into a three-dimensional finite element code to obtain the deformation of the ocular surface under the tear film pressure. The pressure developed in the tear film during blinking was applied as a boundary condition on the ocular surface. Note that the boundary condition (pressure of the tear film) is here unknown and depends on the deformations of the ocular surface and the hydrogel eyelid.

The elastic constants E_{ocular} and v_{ocular} required in the ocular surface model were estimated from the literature. Assuming the engineered tissue had high-water content, we modeled the ocular surface as a nearly incompressible material with a Poisson's ratio v_{ocular} = 0.49. We also used the Young's modulus of the human cornea to estimate E_{ocular} in our model. The Young's

modulus of the human cornea has been measured in various studies[4-6]. For low strains, Hiortdal[5] estimated the Young's modulus of the human cornea to be 3 MPa which we took as the Young's modulus of the ocular surface E_{ocular} in our model.

2. Eyelid
We also considered the hydrogel eyelid as a deformable material whose deformations can be mathematically described using a mattress linear elastic foundation model (also known as the Winkler model)[6]. In this model, the pressure P is linearly related to the deformation of the hydrogel eyelid (in the X-direction) Δh_{eyelid} as

$$\Delta h_{\text{eyelid}} = \frac{P}{K_{\text{eyelid}}} \tag{9}$$

where K_{eyelid} (Nm^{-3}) is the stiffness constant of the hydrogel eyelid. In contact problems, K_{eyelid} can be related to the Young's modulus of the hydrogel eyelid E_{eyelid} as follows[7]

$$\frac{1}{K_{\text{eyelid}}} = \frac{a}{C_{\text{m}}} \frac{\left(1 - v_{\text{eyelid}}^2\right)}{E_{\text{eyelid}}} \tag{10}$$

where v_{eyelid} is the Poisson's ratio of the hydrogel eyelid, C_{m} is a constant, and a is the length of the region in which the eyelid is brought in close proximity to the ocular surface (proximity region)[8]. Substituting Eq. (10) into Eq. (9), the deformation of the hydrogel eyelid (in the X-direction) is determined by

$$\Delta h_{\text{eyelid}} = \frac{a}{C_{\text{m}}} \frac{\left(1 - v_{\text{eyelid}}^2\right)}{E_{\text{eyelid}}} P \tag{11}$$

From Eq. (11), one can note that the normal deformation of the hydrogel eyelid is coupled with the tear film pressure and subsequently with the deformation of the ocular surface.

Based on the one-dimensional model of[8], we modeled the undeformed eyelid wiper as a deformable material with a parabolic profile in the lubrication region

$$h_{\text{eyelid}}^{\text{undeformed}} = h_0 + \frac{Y^2}{R} \tag{12}$$

where $h_{\text{eyelid}}^{\text{undeformed}}$ is the profile of the undeformed eyelid wiper in the lubrication region. Taking the deformation of the eyelid wiper, Δh_{eyelid}, into account, the profile of the deformed eyelid wiper is defined as

$$h_{\text{eyelid}}^{\text{deformed}} = h_0 + \frac{Y^2}{R} + \Delta h_{\text{eyelid}} \tag{13}$$

where h_0 is the minimum of the undeformed eyelid wiper along the Y-axis (see reference[8]) and R is the curvature radius of the undeformed eyelid wiper. Note that h_0 represents the minimum thickness of the tear film when we neglect the deformations of the hydrogel eyelid and the engineered ocular surface.

The Young's modulus of the hydrogel eyelid E_{eyelid} is measured to be 20 kPa. We considered the hydrogel eyelid as a nearly incompressible material with a Poisson's ratio v_{ocular} = 0.49[8]. Based on the Hertz contact theory[7], C_{m} = 1.18 as the undeformed eyelid wiper has a parabolic profile. We set a = 0.7 mm which is approximately the width of the proximity region ("proximity width" shown in the diagram below and **Fig. 3h**). Note that we define the proximity region in our model as a region where the calculated tear film pressure, P, is positive and higher that 0.6 kPa, which is the clinically measured lowest pressure in the human eye[9,10].

3. Tear film

We assumed that the tear film is incompressible, homogenous, and Newtonian. Based on the standard thin film lubrication theory[11], we developed a hydrodynamic model for the tear film dynamics. In this model, the blink-induced pressure P in the tear film was mathematically described by the stationary Reynolds lubrication equation

$$\nabla_{\text{T}} \cdot \left(-\frac{h^3}{12\mu} \nabla_{\text{T}} P + \frac{h}{2} V \right) = 0 \tag{14}$$
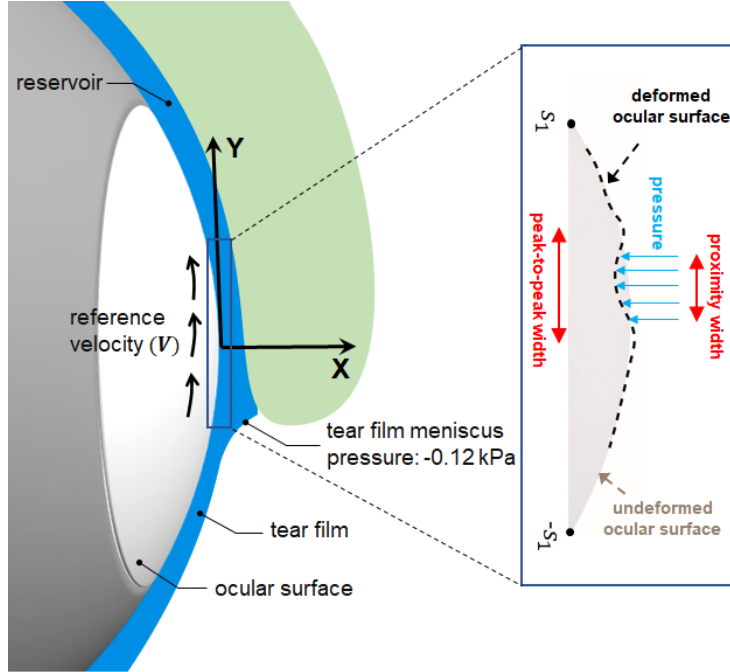
where μ is the viscosity of the tear film, h is the tear film thickness, V is the vector velocity of the reference surface as shown at left, and ∇_{T} is the tangential surface gradient operator (projection of the gradient operator ∇ to the ocular surface). In the derivation of Eq. (14), we neglected the effect of gravity[8] and the variation of the pressure along the tear film thickness[11]. We also applied no-slip boundary conditions at the interfaces of the tear film with the ocular surface and eyelid. We assumed that the tear film viscosity μ did not change with the blink-induced tear film pressure P. As depicted in the diagram, we analyze the tear film flow in a reference configuration where the reference (base) surface moves in the tangential direction s with the same magnitude of the eyelid velocity. As shown in the diagram, the tear film fills the gap between the ocular surface and eyelid. Therefore, the tear film thickness h depends on the tear film pressure P and is given by

$$h = h_{\text{eyelid}}^{\text{deformed}} + |\Delta h_{\text{ocular}}| \tag{15}$$

where Δh_{ocular} is the deformation of the ocular surface in the X-direction (due to the blink-induced pressure) as shown in **Fig. 3j**. It should be noted that all mechanical forces in our model are transmitted to the ocular surface through the tear film. Therefore, h is a key parameter that represents a resultant tear film thickness determined by the combined effects of the movement of the eyelid and other mechanical factors not explicitly described in our model,

9

such as the contractile activity of eyelid muscles. The stationary Reynolds equation (14) requires two boundary conditions

$$P(s = s_1) = P_{\text{reservoir}} \tag{16}$$

$$P(s = -s_1) = P_{\text{meniscus}} \tag{17}$$

where $P_{\text{reservoir}}$ and P_{meniscus} are the pressures in the reservoir and meniscus, respectively. As shown in the diagram, we refer to the region $s > s_1$ as the reservoir wherein the pressure is assumed to be constant along the tangential direction s. As in the previous study[8], we assumed that the reservoir pressure was equal to the atmospheric pressure. Thus, we set $P_{\text{reservoir}} = 0$ in our model since all pressure values were measured relative to the atmospheric pressure. We also assumed that the pressure at $s = -s_1$ was the pressure of the tear film meniscus[10] which can be given by

$$P_{\text{meniscus}} = -\frac{\gamma}{R_{\text{meniscus}}} \tag{18}$$

where γ is the surface tension of the tear film and R_{meniscus} is the curvature radius of the tear film meniscus. The surface tension of human tears has been estimated to be γ = 42-46 mN/m[12]. The radius of curvature of tear meniscus in normal human eyes has been also reported to be R_{meniscus} = 0.365 ± 0.153 mm[13]. Substituting γ = 44 mN/m and R_{meniscus} = 0.365 mm into Eq. (18), the pressure in the tear film meniscus was approximately P_{meniscus} = − 0.12 kPa which was a negligible value compared to the maximum blink-induced tear film pressure of 1.9 kPa shown in **Fig. 3h**. Therefore, we assumed that the tear film pressure outside of the lubrication region ($s > s_1$ and $s < -s_1$) was negligible. The pressure induced in the tear film during blinking is counterbalanced by the normal force F_N that the eyelid exerts to the ocular surface

$$\int_{\Omega} P \, dA - F_N = 0 \tag{19}$$

where Ω is the lubrication region. The Reynolds equation of the tear film (Eq. (14)) coupled with the constitutive equations of the deformable bodies (the ocular surface Eq. (7) and eyelid wiper Eq. (11)) was numerically solved in conjunction with the integral constraint (Eq. (19)) using finite element method.

The constant parameters μ, $|V|$, and F_N required in the tear film model were directly taken from our experimental model. The viscosity of the tear film μ used in our experimental model was estimated to be 1.3 X 10^{-3} Pa·s[14]. The eyelid velocity required in the theoretical tear film model was taken from our experimental measurements shown in **Fig. 3b** where the vertical velocity (in the Y-direction) of the hydrogel eyelid was recorded at different locations as it moved over the ocular surface during the closing phase of a blink. Based on our experimental measurements shown in **Fig. 3b**, the tangent velocity (in the s-direction) of the eyelid was $|V|$ = 125 mm/s when the eyelid was half closed during the down phase of a blink. We also measured the normal force F_N using a piezo-resistive pressure sensor and found that the engineered eyelid exerts the normal force F_N = 8 mN to the ocular surface.

Supplementary Table

List of primary and secondary antibodies

Markers	Primary antibody	Secondary antibody
p63	Rabbit polyclonal anti-CKAP4/p63 antibody (NBP1-85572, Novus)	Goat anti-rabbit IgG H&L (Alexa Fluor® 488) (ab150077, Abcam)
Occludin	Alexa Fluor 594 conjugated mouse monoclonal anti-occludin antibody (331594, Invitrogen)	
CK-3/12	Mouse monoclonal anti-cytokeratin 3+12 antibody (ab68260, Abcam)	Goat anti-mouse IgG H&L (Alexa Fluor® 488) (ab150113, Abcam)
CK-19	Rabbit monoclonal anti-cytokeratin 19 antibody (ab52625, Abcam)	Goat anti-rabbit IgG H&L (Alexa Fluor® 488) (ab150077, Abcam)
MUC16	Rabbit monoclonal anti-MUC16 antibody (ab134093, Abcam)	Goat anti-rabbit IgG H&L (Alexa Fluor® 488) (ab150077, Abcam)
Lubricin	Mouse anti-lubricin antibody/proteoglycan 4 (MABT401, Millipore)	Goat anti-mouse IgG H&L (Alexa Fluor® 594) (ab150116, Abcam)
TLR-4	Rabbit polyclonal anti-TLR-4 antibody (ab13867, Abcam)	Goat anti-rabbit IgG H&L (Alexa Fluor® 488) (ab150077, Abcam)
NF-κB	Rabbit polyclonal anti-NF-κB p65 antibody (ab16502, Abcam)	Goat anti-rabbit IgG H&L (Alexa Fluor® 488) (ab150077, Abcam)

References

1   Holzapfel, G. A. Nonlinear Solid Mechanics: A Continuum Approach for Engineering Science. *Meccanica* **37**, 489-490 (2002).
2   Neto, E. A. d. S., Perić, D. & Owen, D. R. J. *Computational Methods for Plasticity: Theory and Applications*. (Wiley, 2008).
3   Hjortdal, J. Ø. Regional elastic performance of the human cornea. *J Biomech* **29**, 931-942 (1996).
4   Orssengo, G. J. & Pye, D. C. Determination of the true intraocular pressure and modulus of elasticity of the human cornea in vivo. *Bull. Math. Biol.* **61**, 551-572 (1999).
5   Elsheikh, A., Wang, D. & Pye, D. Determination of the Modulus of Elasticity of the Human Cornea. *J Refract Surg* **23**, 808-818 (2007).
6   Skotheim, J. M. & Mahadevan, L. Soft lubrication: The elastohydrodynamics of nonconforming and conforming contacts. *Phys. Fluids* **17**, 092101 (2005).
7   Johnson, K. L. *Contact Mechanics*. (Cambridge Univ. Press, 1985).
8   Jones, M. B., Fulford, G. R., Please, C. P., McElwain, D. L. S. & Collins, M. J. Elastohydrodynamics of the Eyelid Wiper. *Bull. Math. Biol.* **70**, 323-343 (2008).
9   Shaw, A. J., Collins, M. J., Davis, B. A. & Carney, L. G. Eyelid pressure and contact with the ocular surface. *Invest. Ophthalmol. Vis. Sci.* **51**, 1911-1917 (2010).
10   *A. J. B. Shaw, thesis, Queensland University of Technology*.
11   Szeri, A. Z. *Fluid Film Lubrication: Theory and Design*. (Cambridge Univ. Press, 1998).
12   Nagyová, B. & Tiffany, J. M. Components responsible for the surface tension of human tears. *Curr. Eye Res.* **19**, 4-11 (2009).
13   Yokoi, N. *et al.* Reflective meniscometry: a non-invasive method to measure tear meniscus curvature. *Br J Ophthalmol* **83**, 92-97 (1999).
14   Vicario-de-la-Torre, M. *et al.* Design and Characterization of an Ocular Topical Liposomal Preparation to Replenish the Lipids of the Tear Film. *Invest. Ophthalmol. Vis. Sci.* **55**, 7839-7847 (2014).